0IO-Shape PCB Trace Negative Group-Delay Analysis

Fayu Wan, Bin Liu, Preeti Thakur, Atul Thakur, Sébastien Lallechere, Rahajandraibe Wenceslas, Blaise Elysée Guy Ravelo

IEEE Access
Multidisciplinary | Rapid Review | Open Access Journal

Received May 19, 2020, accepted May 22, 2020, date of publication May 25, 2020, date of current version June 5, 2020.

Digital Object Identifier 10.1109/ACCESS.2020.2997464

0IO-Shape PCB Trace Negative Group-Delay Analysis

FAYU WAN[1], (Member, IEEE), BIN LIU[1], PREETI THAKUR[2], ATUL THAKUR[2], SÉBASTIEN LALLÉCHÈRE[3], (Member, IEEE), WENCESLAS RAHAJANDRAIBE[4], (Member, IEEE), AND BLAISE RAVELO[1], (Member, IEEE)

[1]School of Electronics and Information Engineering, Nanjing University of Information Science and Technology (NUIST), Nanjing 210044, China
[2]School of Electronics and Information Engineering, Amity University Haryana, Gurgaon 122413, India
[3]Université Clermont Auvergne (UCA), CNRS, SIGMA Clermont, Institut Pascal, 63178 Aubière, France
[4]Aix-Marseille University, CNRS, University of Toulon, IM2NP UMR7334, 13013 Marseille, France

Corresponding author: Blaise Ravelo (blaise.ravelo@nuist.edu.cn)

This work was supported in part by the NSFC under Grant 61971230 and Grant 61601233, in part by the Jiangsu Distinguished Professor Program and Six Major Talents Summit of Jiangsu Province under Grant 2019-DZXX-022, in part by the Postgraduate Research and Practice Innovation Program of Jiangsu Province under Grant SJKY19_0974, and in part by the Priority Academic Program Development of Jiangsu Higher Education Institutions (PAPD) Fund.

ABSTRACT This paper elaborates a negative group delay (NGD) analysis of 0IO-shape printed circuit board (PCB) traces. This circuit topology is originally implemented with a tri-coupled line (3CL) six-port element with the lateral side connected through lossy transmission lines (TLs). After description of the electrical equivalent diagram, the S-matrix model is established. The group delay (GD) is formulated from the transmission coefficient as a function of the 0IO topological parameters. The effectiveness of the GD modelling is verified with a microstrip circuit proof-of-concept (POC). Simulations and measurements, which are in good agreement, confirm the dual-band bandpass NGD behavior of the 0IO POC. The fabricated prototype generates NGD levels better than −1 ns at NGD center frequencies of about 2.2 GHz and 3 GHz. In addition, to this good NGD performance, the 0IO POC operates with a low insertion loss better than 2.5 dB and reflection losses better than 12 dB in the NGD bandwidths.

INDEX TERMS Microwave theory, distributed topology, negative group delay (NGD), tri-coupled line (3CL), modeling.

I. INTRODUCTION

The group delay (GD) is a key parameter in microwave electronic circuit systems. The GD was exploited for design electronic functions as phase shifting [1], antenna arrays [2] and feedforward amplifier [3] etc. To deal with the unexpected GD issue, the extra delay line is regularly used. The compensation consists generally in compensating the unbalanced GD in the RF and microwave components as in feedforward amplifier [4]. However, this classical solution may be penalizing by adding delay line. Furthermore, the delay line structure can also increase the circuit size greatly. To overcome this issue, recently, negative group delay (NGD) circuits are thought to be a good solution to equalize the microwave electronic system delay.

The associate editor coordinating the review of this manuscript and approving it for publication was Giambattista Gruosso.

In [1], the NGD function was applied to phase shifter to generate at and constant phases over a broad bandwidth. A transmission lines loaded active NGD network is introduced in [2] to solve the beam-squinting problem of conventional series-fed antenna arrays. An NGD circuit is used to enhance feedforward amplifier efficiency by eliminating the delay element, which is one of the major sources of efficiency degradation, without affecting the linearization performance [3]. The NGD effect was also used to improve the flatness of power divider [5]. The NGD structure is constructed with a two-way microstrip line power divider with equal power division ratio. The power divider different transmission paths generate NGD effect despite the insertion losses. From above, it can be seen that the NGD circuits have very extensive applications on RF/microwave devices and systems.

The first NGD synthesizers, with microwave passive circuits were proposed in [6], [7] and with very low-frequency

(LF) active circuits were introduced in [8], [9]. The NGD passive circuits using lumped R, L and C elements only work at frequencies lower than 1 GHz [10], [11], limiting the available scope of microwave applications. Since NGD occurs at the range of frequencies where the absorption or the attenuation is maximum, the NGD generation is accompanied by excessive isolation loss more than 20 dB [6], [7]. Therefore, the cascading of active elements such as amplifiers is a practical compensation for these attenuations [12], [13]. Thus, in [13], a field effect transistor (FET) is applied to design an active NGD circuit with 2dB gain. However, it was found that these active NGD circuits would unavoidably suffer from design inflexibility restrictions about the fixed component values and increasing design difficulties in the microwave band. And also, it can increase the out-of-band noise as well as make the circuit more complicated. Moreover, such an active topology is rather complex to design and difficult to integrate because of the lossy lumped inductor.

As a result, simpler and low-loss passive topologies built with distributed transmission lines (TLs) were implemented [12]–[19]. To reduce the attenuation lower than 10 dB, a coupled line based NGD circuit is designed in [16] whose attenuation is decreased to 7.43 dB. A parallel interconnect line (PIL) NGD circuit is designed in [18]. This PIL NGD circuit is able to operate with attenuation of about 5 dB. An NGD circuit consists of the isolated- and coupled-accesses connected in a feedback loop as a coupling between "1" and "0" shape interconnect line which presents 2.4 dB insertion loss [19]. Such geometrical shape as "01O" sensitively with electromagnetic interference (EMI) can be found in the PCB traces.

These "01O" configurations can be found in PCB layouts constituted by copper plane hotspots, vias interconnects, serpentine and twirling paths (for length compensation, pads interconnects, symmetrical breakouts etc.). It would be important to investigate the coupling effect modelling of this structure and the possibility of NGD effect generation. The motivation of this work is to properly assess the impact of NGD generation (quantifying and/or evaluating it) with respect to tri-coupled line EMC (electromagnetic compatibility) and EMI scenarios. When dealing with coupling scenarios involving "01O" structures, it is of utmost importance for the EMC designer to ensure the system functioning taking into account NGD effects. Compared with the existing single-band NGD circuits [12]–[19], [21]–[23], the design of dual-band NGD circuits [24]–[27] remains a challenging task. In order to enable the NGD circuit to operate in different frequency bands, few studies are focused on the design of dual-band NGD circuits. A dual-plane U-shaped defected structure is used to realize a dual band NGD circuit [25], whose first center frequency and second center frequency are determined by a defected microstrip structure (DMS) and a defected ground structure (DGS), respectively. However, the attenuation is worse than 44 dB. A compact dual-band NGD circuit composed of an open-circuited TL and two resistors connected by two TLs is proposed in [27]. The attenuation is worse than 16 dB. Therefore, it is especially important to design a low-loss dual-band NGD circuit.

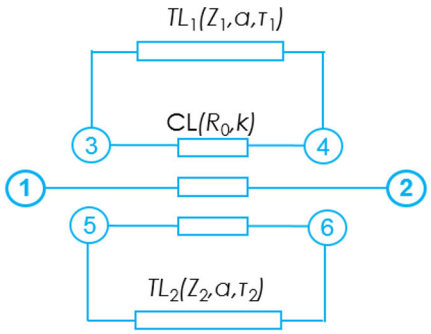

FIGURE 1. Topology of 0IO structure under study.

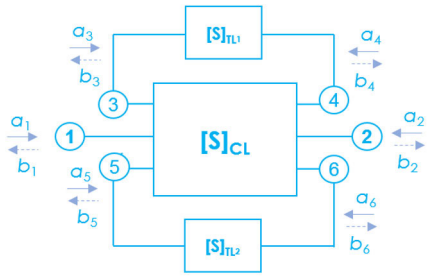

FIGURE 2. S-parameter black blocks-based diagram equivalent to the 0IO topology introduced in Fig. 1.

For this reason, in this paper, a topology of dual band NGD passive topology based on fully distributed TLs with further challenge on TL loss and delay effect is developed. The challenging NGD topology presents an innovative shape similar to "0IO" shape geometry. The topology is built with a tri-coupled line (3CL) six-port element with the lateral side connected through lossy transmission lines (TLs). The paper is mainly organized in four different sections as follows:

- The theoretical approach allowing to model the 0IO topology S-matrix is described in Section II. After the GD modelling, the NGD analysis is introduced.
- The validity of the bandpass NGD functioning of the 0IO topology is validated in Section III via excellent comparisons between calculation, simulation and measurement.
- Finally, Section IV concludes the paper.

II. NGD THEORETICAL INVESTIGATION ON "0IO" TOPOLOGY

The present section is focused on the NGD theoretical approach of the 0IO topology. The S-matrix model is established from wave power interactions between the topology constituting elements. The GD expression is derived from the transmission coefficient. Then, NGD analysis is introduced in function of the 0IO parameters.

A. DESCRIPTION OF THE 0IO TOPOLOGY

Fig. 2 sketches the topology of 0IO structure under study. It is comprised mainly of a six-port tri-coupled line (3CL) denoted

CL(R_0, k) having characteristic impedance $R_0 = 50\ \Omega$ and the adjacent line coupling coefficient k. We suppose that the coupling between line TL③–④ and TL⑤–⑥ are negligible. The main access ports are constituted by ① and ②.

The lateral lines are interconnected through different lossy TLs $\mathrm{TL_k}(Z_k, a_k, \tau_k)$ for $k = \{1, 2\}$ which are supposed to be ideal with same characteristic impedances $Z_k = R_0$ and attenuation $a_k = a$. However, they present different propagation delay $\tau_1 < \tau_2$.

After the equivalent circuit introduction, the S-matrix modeling of the 0IO topology will be explored in the next paragraph.

B. S-MATRIX EQUIVALENT MODEL OF 0IO STRUCTURE CIRCUIT

To establish the S-matrix model of the 0IO topology, we propose to consider the equivalent diagram composed of TL_1, TL_2 and CL S-matrix black boxes $[S]_{TL_1}$, $[S]_{TL_2}$ and $[S]_{CL}$ shown in Fig. 2, respectively.

The modelling of our hexapole circuit is built with the consideration of equivalent S-parameters. The main constituting elements are a CL and the four pieces of terminal TLs introduced in Fig. 2. Based on the S-parameter theory, the general S-parameter of the 01O topology can be written in function of the wave powers. The CL six-port S-matrix constituting the central element is linked to the input and output wave powers a_m and b_m ($m = \{1, 2, \ldots, 6\}$) by the relation:

$$\begin{bmatrix} b_1 \\ b_2 \\ b_3 \\ b_4 \\ b_5 \\ b_6 \end{bmatrix} = [S]_{CL} \times \begin{bmatrix} a_1 \\ a_2 \\ a_3 \\ a_4 \\ a_5 \\ a_6 \end{bmatrix}. \tag{1}$$

The main objective of the theoretical approach is to determine the overall equivalent two-dimension S-matrix $[S]_{0IO}$ by reducing this six-dimension matrix. Meanwhile, this total S-matrix can be determined from the constituting TL and CL ones. Substituting the expressions of wave powers a_m and b_m ($m = \{3, \ldots, 6\}$) into (1), the overall S-matrix is defined by the relation:

$$\begin{bmatrix} b_1 \\ b_2 \end{bmatrix} = [S] \times \begin{bmatrix} a_1 \\ a_2 \end{bmatrix}. \tag{2}$$

1) S-MATRIX OF CL ELEMENT

According to the coupler theory, the CL S-matrix can be written in function of the two-neighboring lines coupling (between ports ①-③, ①-⑤, ②-④ and ②-⑥) k and direct transmission (between ports ①-② , ③-④ and ⑤-⑥):

$$k_0 = -j\,g = -j\sqrt{1 - k^2}, \tag{3}$$

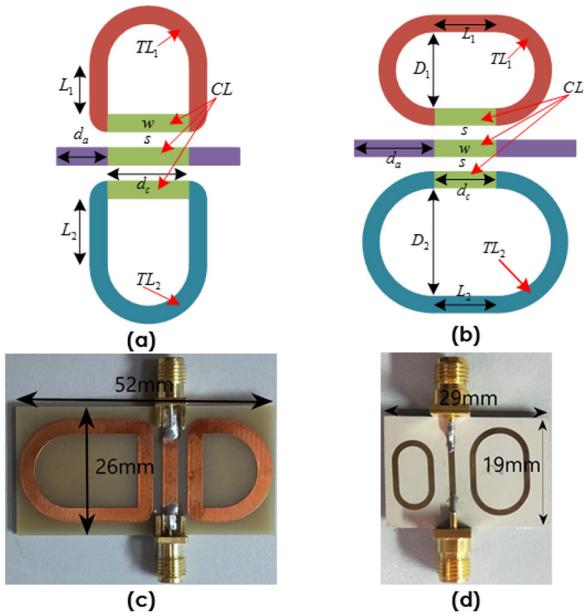

FIGURE 3. 0IO microstrip prototype: (a) ADS® design and (b) photograph.

with the complex number $j = \sqrt{-1}$. Under this hypothesis, the CL S-matrix model is ideally assigned as:

$$[S]_{CL} = \begin{bmatrix} 0 & k_0 & k & 0 & k & 0 \\ k_0 & 0 & 0 & k & 0 & k \\ k & 0 & 0 & k_0 & 0 & 0 \\ 0 & k & k_0 & 0 & 0 & 0 \\ k & 0 & 0 & 0 & 0 & k_0 \\ 0 & k & 0 & 0 & k_0 & 0 \end{bmatrix}. \tag{4}$$

2) S-MATRIX MODEL OF TL1,2

Following the topological description introduced in Fig. 3, the $\mathrm{TL_k}$ for $k = \{1, 2\}$ S-matrices are linked to the wave powers by the relation:

$$\begin{cases} \begin{bmatrix} a_3 \\ a_4 \end{bmatrix} = [S]_{TL_1} \times \begin{bmatrix} b_3 \\ b_4 \end{bmatrix} \\ \begin{bmatrix} a_5 \\ a_6 \end{bmatrix} = [S]_{TL_2} \times \begin{bmatrix} b_5 \\ b_6 \end{bmatrix}. \end{cases} \tag{5}$$

By denoting ω is the angular frequency variable, let us take:

$$x(j\omega) = a\,e^{-j\omega\tau_k}. \tag{6}$$

Therefore, the equivalent TL_1 and TL_2 S-matrices can be written as:

$$[S(j\omega)]_{TL_k} = \begin{bmatrix} 0 & x_k(j\omega) \\ x_k(j\omega) & 0 \end{bmatrix}. \tag{7}$$

3) EXPRESSION OF 0IO STRUCTURE GLOBAL S-MATRIX

It can be derived from (4) and (6) that wave powers a_m and b_m ($m = \{3, \ldots, 6\}$) can be expressed in function of $a_{1,2}$ and

$b_{1,2}$. Substituting the according equations into (1) combined with (4), the 0IO S-matrix introduced in (2) is written as:

$$[S(j\omega)] = \begin{bmatrix} 0 & S_{21}(j\omega) \\ S_{21}(j\omega) & 0 \end{bmatrix} \tag{8}$$

with the transmission coefficient:

$$S_{21}(j\omega) = \frac{\begin{array}{c} x_1(j\omega) + x_2(j\omega) \\ +j\,g\left[(1+k^2)x_1(j\omega)x_2(j\omega) - 1\right] \end{array}}{\left[1 + j\,g\,x_1(j\omega)\right]\left[1 + j\,g\,x_2(j\omega)\right]}. \tag{9}$$

Based on this last expression, the NGD analysis is introduced in the next subsection.

C. ANALYSES OF S-MATRIX FREQUENCY RESPONSES

The transmission coefficient magnitude, $S_{21}(\omega) = |S_{21}(j\omega)|$, can be formulated as:

$$S_{21}(\omega) = \frac{\sqrt{\begin{array}{l} \left\{\begin{array}{l} a\left[\cos(\omega\tau_1) + \cos(\omega\tau_2)\right] \\ +g\sin\left[\omega(\tau_1+\tau_2)\right] \end{array}\right\}^2 \\ +\left\{\begin{array}{l} a\left[\sin(\omega\tau_1) + \sin(\omega\tau_2)\right] \\ +g\left\{a^2(1+k^2) - \cos\left[\omega(\tau_1+\tau_2)\right]\right\} \end{array}\right\}^2 \end{array}}}{\sqrt{\begin{array}{l} \left\{\begin{array}{l} \cos\left[\omega(\tau_1+\tau_2)\right] + \sin\left[\omega(\tau_1+\tau_2)\right] \\ -a^2g^2 - a\,g\left[\sin(\omega\tau_1) + \sin(\omega\tau_2)\right] \end{array}\right\}^2 \\ +\left\{\begin{array}{l} a\,g\left[\cos(\omega\tau_1) + \cos(\omega\tau_2)\right] + \\ \sin\left[\omega(\tau_1+\tau_2)\right] \end{array}\right\}^2 \end{array}}}. \tag{10}$$

The transmission phase is defined by:

$$\varphi(\omega) = \angle S_{21}(j\omega) = \varphi_n(\omega) - \varphi_d(\omega) \tag{11}$$

with

$$\varphi_n(\omega) = \arctan\left\{\frac{\begin{array}{c} a\left[\sin(\omega\tau_1)+\sin(\omega\tau_2)\right] \\ +g\left\{a^2(1+k^2)-\cos\left[\omega(\tau_1+\tau_2)\right]\right\} \end{array}}{\begin{array}{c} a\left[\cos(\omega\tau_1)+\cos(\omega\tau_2)\right] \\ +g\sin\left[\omega(\tau_1+\tau_2)\right] \end{array}}\right\} \tag{12}$$

$$\varphi_d(\omega) = \arctan\left\{\frac{\begin{array}{c} a\,g\left[\cos(\omega\tau_1)+\cos(\omega\tau_2)\right] \\ +\sin\left[\omega(\tau_1+\tau_2)\right] \end{array}}{\begin{array}{c} \cos\left[\omega(\tau_1+\tau_2)\right]+\sin\left[\omega(\tau_1+\tau_2)\right] \\ -a^2g^2 - a\,g\left[\sin(\omega\tau_1)+\sin(\omega\tau_2)\right] \end{array}}\right\}. \tag{13}$$

D. NGD ANALYSIS OF 0IO STRUCTURE

The 0IO topology GD is defined from the transmission phase expressed in (11) with the equation:

$$\tau(\omega) = \frac{-\partial\varphi(\omega)}{\partial\omega}. \tag{14}$$

Thanks to equations (12) and (13), we can rewrite this GD as follows:

$$\tau(\omega) = \tau_d(\omega) - \tau_n(\omega) \tag{15}$$

with:

$$\tau_n(\omega) = \frac{\partial\varphi_n(\omega)}{\partial\omega} \tag{16}$$

and

$$\tau_d(\omega) = \frac{\partial\varphi_d(\omega)}{\partial\omega}. \tag{17}$$

In details, the phase numerator GD is given by:

$$\tau_n(\omega) = \frac{\begin{array}{c} (\tau_1+\tau_2)\left\{\xi_1 + \left[\xi_2 + \xi_3\cos(\omega\tau_1)\right]\sin(\omega\tau_2)\right\} \\ +\left[\xi_4 + \xi_5\sin(\omega\tau_2)\right]\sin(2\omega\tau_1)/2 \end{array}}{\begin{array}{c} \upsilon_1 + \left[\upsilon_2 + \upsilon_3\cos(\omega\tau_1)\right]\sin(\omega\tau_2) \\ +\left[\upsilon_4 + \upsilon_5\sin(\omega\tau_2)\right]\sin(2\omega\tau_1)/2 \end{array}} \tag{18}$$

with:

$$\begin{cases} \xi_1 = a^2k^4\cos(\omega\tau_2) \\ \xi_2 = g^2 + a^2 \\ \xi_3 = a\,g\left\{2\tau_1 + \left[1 + a^2(1+k^2)\right]\tau_2\right\} \\ \xi_4 = a\,g\left\{\left[1 + a^2(1+k^2)\right]\tau_1 + 2\tau_2\right\} \\ \xi_5 = a^2g^2(\tau_1+\tau_2) \end{cases} \tag{19}$$

$$\begin{cases} \upsilon_1 = 2a^2k^4\cos(\omega\tau_2) \\ \upsilon_2 = a^2 + g^2\left[1 + a^4(1+k^2)\right] \\ \upsilon_3 = 2a\,g(1+a^2+k^2) \\ \upsilon_4 = 2a^2g^2. \end{cases} \tag{20}$$

The phase denominator GD is expressed as:

$$\tau_d(\omega) = \frac{\begin{array}{c} \left[(1+a^2g^2)\tau_1 + 2\tau_2\right]\left[\chi_1 + a\,g\sin(\omega\tau_1)\right] \\ +a\,g(\tau_1+\tau_2)\sin(\omega\tau_2)\left[\chi_2 + a^2g^2\sin(\omega\tau_1)\right] \end{array}}{\begin{array}{c} \left[1 + a^2g^2 + 2a\,g\sin(\omega\tau_1)\right] \\ \left[1 + a^2g^2 + 2a\,g\sin(\omega\tau_2)\right] \end{array}} \tag{21}$$

with:

$$\begin{cases} \chi_1 = (1+a^2g^2)\tau_1 + 2\tau_2 \\ \chi_2 = 2\tau_1 + (1+a^2g^2)\tau_2. \end{cases} \tag{22}$$

Based on these analytical expressions, parametric analyses versus TL delays $\tau_{1,2}$ where performed to visualize the NGD effect. More importantly, simulations and experimental studies with a POC were also realized. The obtained validation results will be explored in the next section.

III. EXPERIMENTAL VALIDATIONS WITH 0IO PROTOTYPES

As application of the previous theory, a prototype of 0IO POC has been designed, simulated and fabricated. The obtained results will be discussed in the next paragraph.

A. DESCRIPTION OF CONSIDERED 0IO NGD PROTOTYPES

To verify the relevance of the previous theory, 0IO POCs were designed and simulated with ADS®. The designed and photographed two-port circuits based on:

- FR4-epoxy substrate are viewed in Fig. 3(a) and in Fig. 3(c),
- and based on Rogers substrate are shown in Fig. 3(b) and in Fig. 3(d), respectively.

The designed circuits were simulated in the ADS® environment. We can see in these designs the lateral delay lines

TABLE 1. Parameters of the 0IO prototype shown in Figs. 3(a) and 3(c).

Components	*Description*	*Parameter*	*Value*
Dielectric substrate (FR4)	Relative permittivity	ε_r	4.4
	Loss tangent	$\tan(\delta)$	0.02
	Thickness	h	1.6 mm
Metallization (Cu)	Conductor thickness	t	35 µm
	Conductivity	σ	58 MS/m
Feedback line TL_1	Physical length	d_1	40 mm
	Attenuation loss	a_1	-0.2 dB
	Delay	τ_1	0.24 ns
	partial length	L_1	3.515 mm
Feedback line TL_2	Length	d_2	40 mm
	Attenuation	a_2	-0.2 dB
	Delay	τ_2	0.37 ns
	partial length	L_2	13.515 mm
Coupled CL	Width	w	3 mm
	Length	d_3	15 mm
	Interspace	s	2 mm
	Coupling coefficient	k	-21 dB
Access lines	Width	w	3 mm
	Physical length	d_4	10 mm

TABLE 2. Parameters of the 0IO prototype shown in Fig. 3(b) and Fig. 3(d).

Components	*Description*	*Parameter*	*Value*
Dielectric substrate (Rogers3210)	Relative permittivity	ε_r	10.2
	Loss tangent	$\tan(\delta)$	0.0027
	Thickness	h	1.27 mm
Metallization (Cu)	Conductor thickness	t	35 µm
	Conductivity	σ	58 MS/m
Feedback line TL_1	partial length	L_1	40 mm
	diameter	D_1	5.39 mm
Feedback line TL_2	partial length	L_2	6 mm
	diameter	D_2	8.85 mm
Coupled CL	Width	w	1.09 mm
	Length	dc	6 mm
	Interspace	s	2.7 mm
Access lines	Width	w	1.09 mm
	Physical length	d_4	6 mm

and the middle CL. Additional access lines TL_3 and TL_4 are added in order to facilitate the measurement configuration. The pictures of the 0IO POC prototype are shown in Fig. 3(c) and Fig. 3(d). These prototypes are implemented in microstrip technology without use of lumped and lossy component. The physical parameters of the FR4 and Rogers substrate 0IO circuit prototypes are indicated in Tables 1 and 2, respectively. The conductor lines are Cu-metallized. The physical sizes of constituting distributed lines TL_1, TL_2 and CL are also indicated in Table 1. The associated electrical parameters as characteristic impedances, delay and coupling coefficient calculated from ADS® LineCalc microwave circuit calculation tool are also given in this table.

Based on this prototype, validation studies were performed with parametric analyses with respect to the TL lengths.

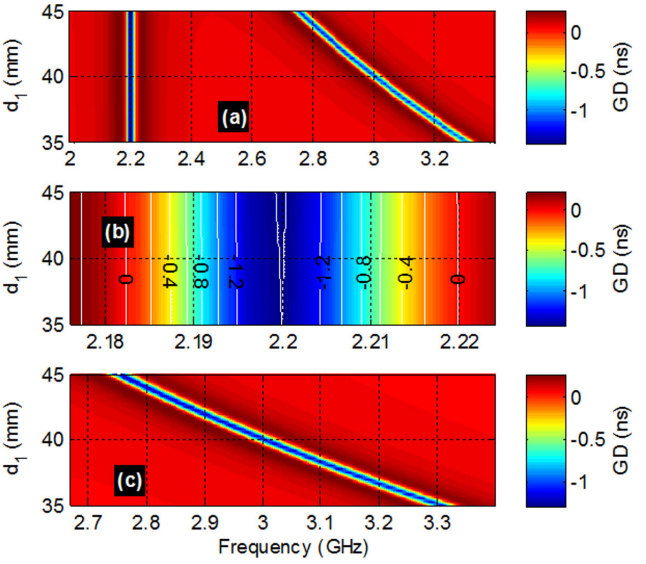

FIGURE 4. GD parametric analysis with respect to TL_1 physical length d_1: (a) wideband, and around (b) the 1st and (c) 2nd NGD BWs.

Furthermore, practical investigation with experimental testing will be discussed in the following subsection.

B. PARAMETRIC ANALYSES

To get a predictive insight about the bandpass NGD behavior of the 0IO topology, parametric analyses with respect to TL_1 and TL_2 delays τ_1 and τ_2, by means of physical lengths d_1 and d_2 were computed with S-parameter simulations from 2 GHz to 3.4 GHz. The obtained results are explored in the following paragraphs.

1) INFLUENCE OF TL_1 DELAY

The influence of TL_1 delay is studied with parametric simulations by varying physical length d_1 from 35 mm to 45 mm. Fig. 4(a) exposes the GD map versus frequency and d_1. This result reveals that the 0IO topology behaves as a dual-band bandpass NGD function. Two NGD bandwidths (BWs) can be identified. The first NGD BW situated around 2.2 GHz is zoomed in Fig. 4(b).

It shows an NGD function that is not sensitive to d_1 variation. It means that this NGD bandwidth should depend to the loop related to TL_2 and therefore, it must be linked to delay τ_2. The second NGD BW area, situated between 2.73 GHz and 3.33 GHz is displayed in Fig. 4(c). This NGD BW varies inversely with delay τ_1. Therefore, we denote f_1 the NGD center frequency associated to this second NGD bandwidth.

The analytical relations between the two NGD center frequencies $f_{1,2}$ and delays τ_1 can be understood more clearly with the graphical plots of Fig. 5(a). At these NGD center frequencies, NGDs are approximately estimated as $GD(f_1)$ varying between -1.3 ns and -1.2 ns, and $GD(f_2) \approx -1.4$ ns. In addition to the GD analysis, the S_{21} variation with respect to d_1 is displayed in Figs. 6. The low loss aspect with insertion

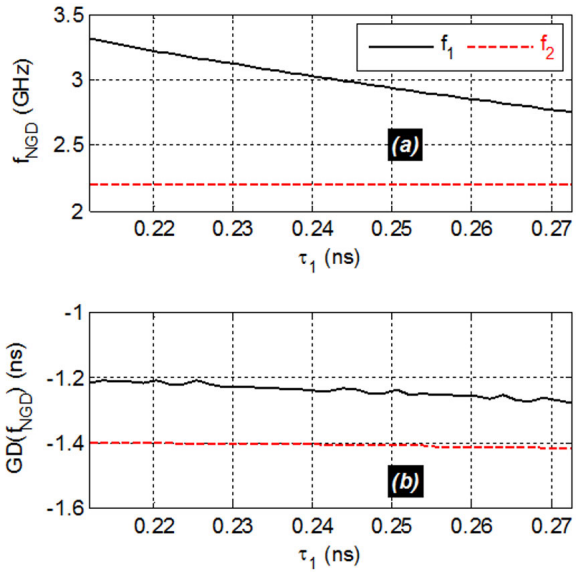

FIGURE 5. (a) NGD center frequencies $f_{1,2}$ and (b) GD($f_{1,2}$) versus τ_1.

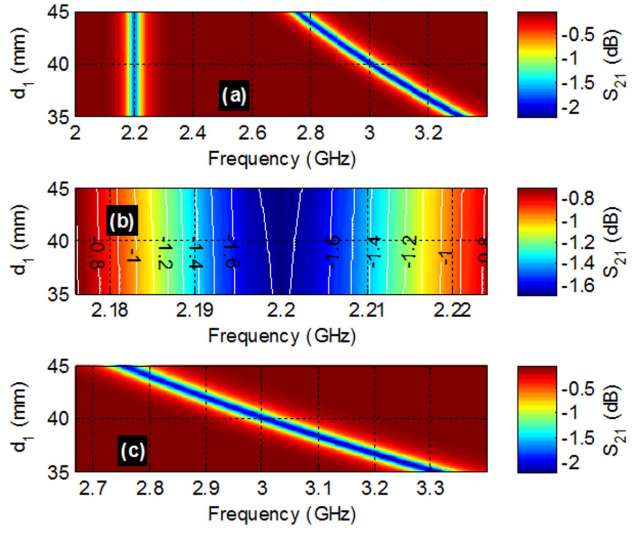

FIGURE 6. $S_{12} = S_{21}$ parametric analysis with respect to TL_1 physical length d_1: (a) wideband, and around (b) the 1st and (c) 2nd NGD BWs.

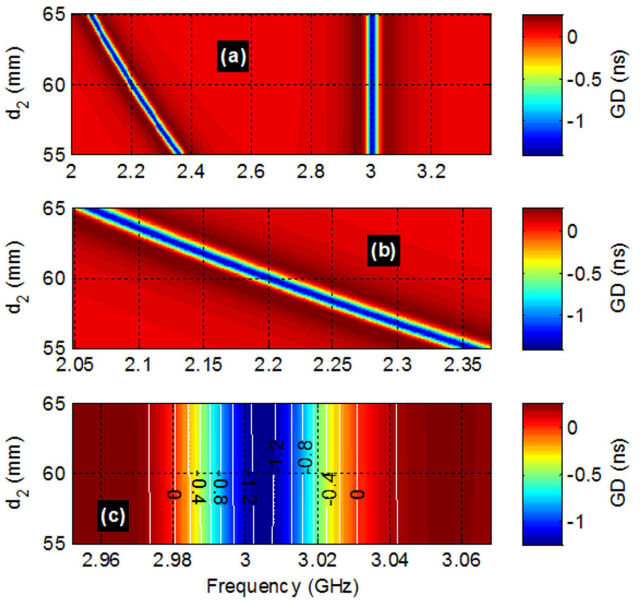

FIGURE 7. GD parametric analysis with respect to TL_2 physical length d_2: (a) wideband, and around (b) the 1st and (c) 2nd NGD bandwidth.

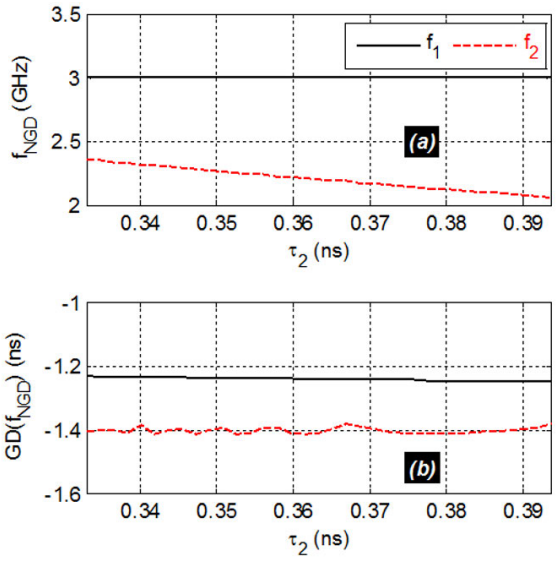

FIGURE 8. (a) NGD center frequencies $f_{1,2}$ and (b) GD($f_{1,2}$) versus τ_2.

loss lower than 2.5 dB is explained by the wide frequency range mapping in Fig. 6(a). It can be underlined that the insertion loss presents a similar behavior as the GD shown in Figs. 4. The insertion loss in the first NGD bandwidth is insensitive to the variation of d_1.

2) INFLUENCE OF TL_2 DELAY

Similar to the previous case of study, parametric analyses with respect to d_2 varied from 55 mm to 65 mm were realized to investigate the influence of TL_2 delay τ_2.

Fig. 7(a) displays the maps of GD from 2 GHz to 3.4 GHz. This map reveals that the first NGD BW with center frequency f_2 is sensitive to delay τ_2.

As mapped in Fig. 7(b) and plotted in Fig. 8(a), the NGD center frequencies $f_1 \approx 3$ GHz and f_2 varies between 2 GHz and 2.4 GHz. As seen in Fig. 8(b), the associated GDs are approximately equal to $\tau_1 \approx -1.25$ ns and $\tau_2 \approx -1.4$ ns. Figs. 9 display the maps of transmission coefficient versus frequency and τ_2. Once again, the map behaviors are similar to the GD and shows that only the first NGD BW is sensitive to τ_2.

C. INVESTIGATION ON SIMULATED AND EXPERIMENTAL RESULTS

To complete the validation, practical analysis of 0IO NGD prototype was investigated via S-parameter measurement

TABLE 3. Simulated and measured NGD specifications of the FR4 substrate based prototype shown in Fig. 3(a) and Fig. 3(c).

Approach	f_1 (GHz)	$\tau(f_1)$ (ns)	BW (MHz)	$S_{21}(f_1)$ (dB)	$S_{11}(f_1)$ (dB)	f_2 (GHz)	$\tau(f_2)$ (ns)	BW (MHz)	$S_{21}(f_2)$ (dB)	$S_{11}(f_2)$ (dB)
ADS®	2.194	-1.44	31	-1.9	-17	3	-1	45	-2.3	-13
Mom.	2.219	-2.13	26	-2.6	-13	2.988	-1	43	-2.3	-12
Meas.	2.209	-1.43	35	-2.4	-14	2.941	-0.76	53	-2.5	-13

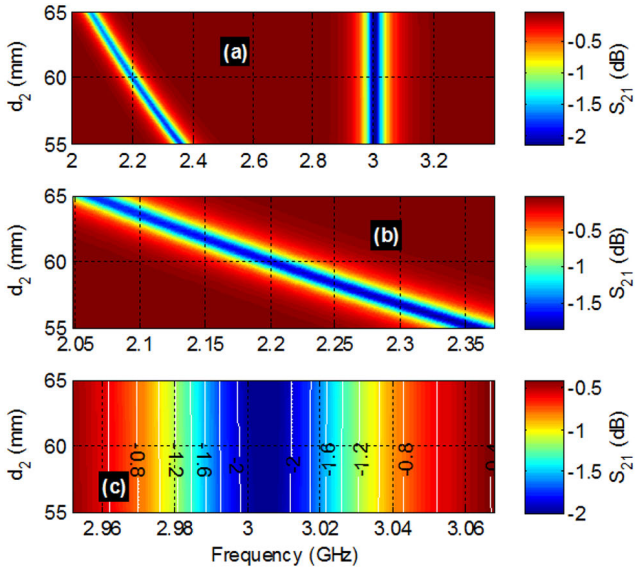

FIGURE 9. $S_{12} = S_{21}$ parametric analysis with respect to the TL_2 physical length d_2: (a) wideband, and around (b) the 1st and (c) 2nd NGD bandwidth.

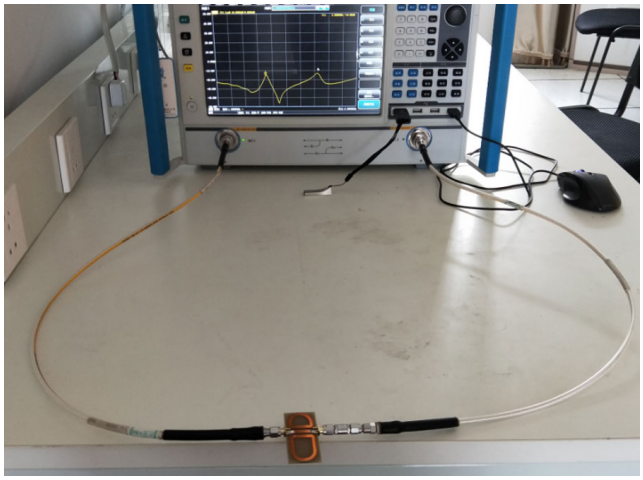

FIGURE 10. S-parameter measurement experimental setup of the 0IO prototype.

from 2 GHz to 3.4 GHz. The experimental setup configuration with vector network analyzer (VNA) is shown in Fig. 10.

The validation study was performed via comparisons of the plots of GDs, transmission and reflection coefficients from measurements (“meas.”), circuit schematic (“schem.”) and EM momentum (“mom.”) simulations from ADS®.

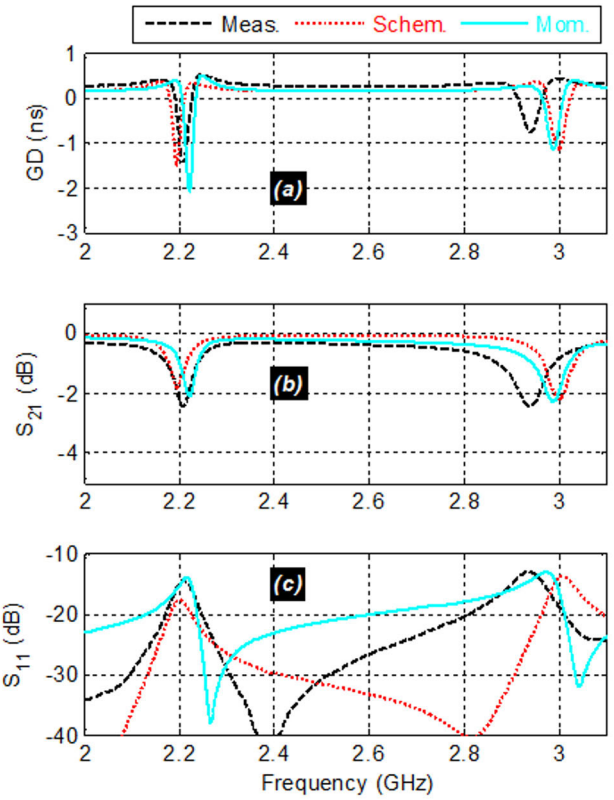

FIGURE 11. Comparisons of measured, ADS schematic, and momentum simulations of: (a) GD, (b) $S_{12} = S_{21}$ and (c) $S_{11} = S_{22}$ from the 0IO prototype shown in Figs. 3(a) and 3(c).

Two different “01O” interconnect prototypes from FR4- and Rogers-substrate based were tested to illustrate the NGD effect possibility.

1) DISCUSSION ON NGD TEST RESULTS OF FR4-BASED 0IO PROTOTYPE

Figs. 11 present the comparison results in the wide frequency range which confirm the dual-band bandpass NGD behavior of FR4 substrate based 0IO prototype. The simulated and measured GD and transmission coefficients of Figs. 11(a) and 11(b), respectively are in very good agreement. However, as shown in Fig.11(c), the simulated and measured reflection coefficients are showing considerable differences of behaviors. These main differences are first of all linked to the low values of reflection coefficient under than −10 dB where the differences seem to be relatively significant but remain negligible in linear valuer.

TABLE 4. Simulated and measured NGD specifications of the rogers substrate based prototype shown in Fig. 3(b) and Fig. 3(d).

Approach	f_1 (GHz)	$\tau(f_1)$ (ns)	BW (MHz)	$S_{21}(f_1)$ (dB)	$S_{11}(f_1)$ (dB)	f_2 (GHz)	$\tau(f_2)$ (ns)	BW (MHz)	$S_{21}(f_2)$ (dB)	$S_{11}(f_2)$ (dB)
ADS®	2.716	-3.34	20	-2.33	-12.82	3.58	-3.9	30	-2.68	-12.89
Meas.	2.725	-3.65	21	-3.17	-10.53	3.568	-1.86	34	-2.81	-14.93

TABLE 5. Performance comparison between the 0IO and other NGD circuits.

References	f (GHz)		BW (MHz)		NGD (ns)		S_{21} (dB)		S_{11} (dB)		Use of lossy resistor
	f_1	f_2	BW_1	BW_2	f_1	f_2	f_1	f_2	f_1	f_2	
[24]	2.1	3.5	180	180	-3	-3.1	-34	-35	-17	-17	Yes
[25]	3.5	5.15	62	59	-4.5	-4.2	-27	-28	N/A(*)	N/A(*)	Yes
[26]	3.5	5.2	200	400	-5	-5	13	20	N/A(*)	N/A(*)	Yes
[27]	0.66	1.39	446	198	-1	-1	16.9	16.9	-18	-17	Yes
This work with FR4-substrate	2.2	2.9	35	43	-1.5	-0.9	-2.2	-2.2	-15	-13	No
This work with Rogers substrate	2.72	3.56	21	34	-3.65	-1.86	-3.1	-2.81	-10.53	-2.81	No

(*) *N/A: Not Applicable*

In the all parameters (the GD, transmission and reflection coefficients), the observed discrepancies between simulated and measured results plotted in Figs. 11 are mainly due to:

- The fabrication errors related to the microstrip line width, lengths and connectors,
- The measurement uncertainties,
- The full wave simulation inaccuracies linked to the meshing and iterative computations,
- And also the FR4-epoxy substrate material parameter uncertainties as the relative permittivity, and loss tangent.

As indicated in comparative Table 3, the NGD center frequencies are localized around 2.2 GHz and 3 GHz. To highlight the NGD behaviors, the zoom in plot around the NGD narrow BWs are depicted in Figs. 12. It can be seen that the FR4 substrate based 0IO prototype presents an NGD BWs of about 35 MHz and 53 MHz. The slight shifts and differences between the NGD central frequency and values shift between the simulated and measurement results is due to the tolerance of the considered dielectric substrate effective permittivity. Moreover, similar to all microwave circuits, the 0IO NGD specifications must include the insertion and reflection losses. As seen in Fig. 11(b), the NGD 0IO prototype presents maximal attenuation of only 2.5 dB around the NGD center frequency. The S-parameters plotted in Fig. 11(c) confirm that the reflection losses are better than 12 dB in the NGD BWs.

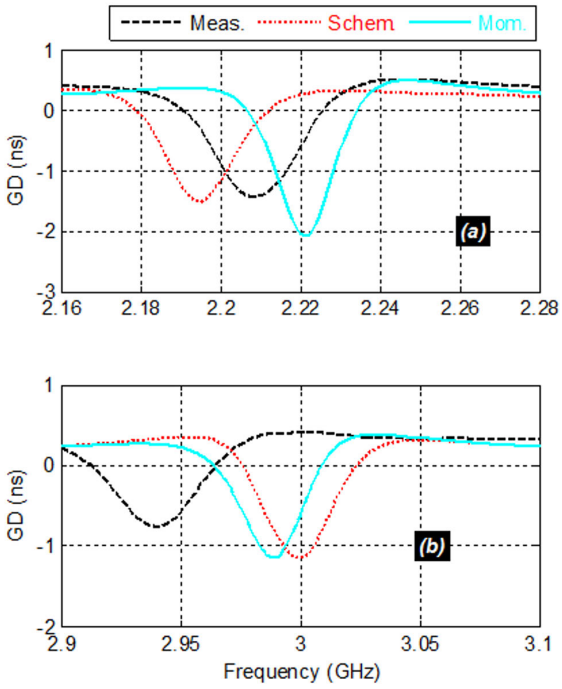

FIGURE 12. Zoom in of measured and simulated GDs around the (a) 1st and (b) 2nd NGD BWs.

2) DISCUSSION ON NGD TEST RESULTS OF ROGERS-BASED 0IO PROTOTYPE

A good correlation between simulated and measured results is realized with Rogers substrate based "0IO" prototype introduced in Fig. 3(b) and Fig. 3(d). Once again, it can be seen that the circuit generates the dual-band NGD effect with center frequencies of about $f_1 = 2.71$ GHz and $f_2 = 3.58$ GHz as shown in Figs. 13(a).

Despite the slight differences indicated in Table 4, the transmission and reflection coefficients as reported

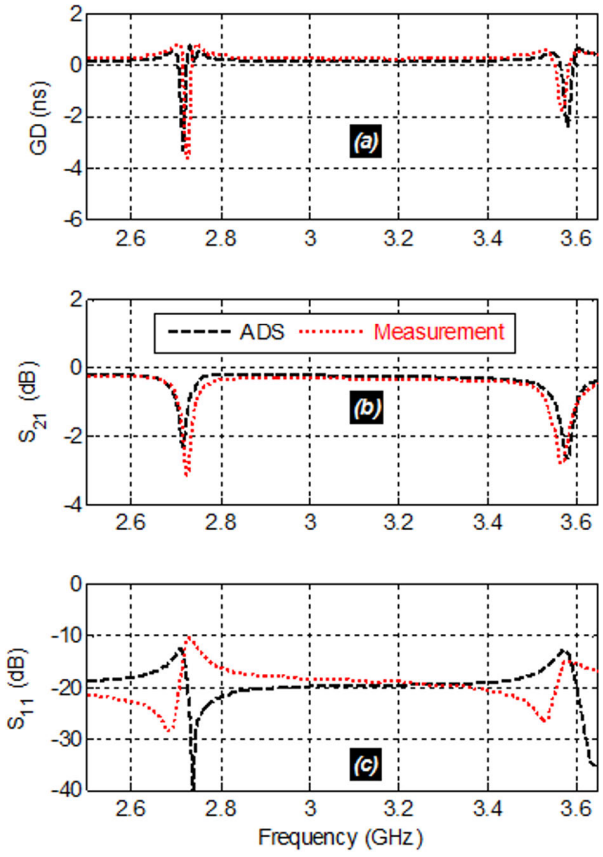

FIGURE 13. Measured and simulated GDs around the (a) 1st and (b) 2nd NGD BWs from the 0IO prototype shown in Fig. 3(b) and 3(d).

in Fig. 13(b) and in Fig. 13(c), respectively are also in very good agreement notably in the NGD bandwidth. The same as in the results of previous case based on Figs. 11, the slight differences between simulated and measured results plotted in Figs. 13(c) are mainly caused by the imperfections of simulated and NGD circuit prototype fabrications.

To point out the innovative advantages of the 0lO structures, comparative study on NGD performance is addressed in the next subsection.

D. DISCUSSION ON NGD PERFORMANCES

The NGD passive performances of tested 0IO structures are, particularly interesting, compared to the existing dual-band NGD circuits proposed in [24]–[27]. Table 5 summarizes the comparison between the NGD, insertion and reflection loss performances including the dual-band NGD bandwidth. It can be pointed out that the 0IO-shape circuit allows to achieve a very good attenuation showing low-loss aspect under very good reflection coefficient. Moreover, compared to the NGD circuits designed in [24]–[27], the 0IO-shape circuit is merely built with a fully distributed circuit without using any lossy lumped element as resistor.

IV. CONCLUSION

An innovative NGD analysis of particular 0IO-shape PCB traces is investigated. The proposed topology consists originally of 3-CL with lateral side interconnect in feedback with lossy and delayed different TLs. The S-matrix model of this particular NGD topology is established. Then, the NGD analysis is presented by exploiting the GD through the transmission coefficient expression. The NGD theoretical approach was validated by designing fully distributed microstrip structures without lumped elements even a resistance. Therefore, an NGD bandpass behavior is realized. A very good agreement between the simulations and measured S-parameters and GDs are realized.

The investigated "0IO" topology is promising for future RF and microwave system applications with the possibility to operate with low attenuation and reflection losses. This solution is utmost importance for the electronic systems designers, ensuring the system functioning jointly with PCB layout guidelines.

REFERENCES

[1] B. Ravelo, M. Le Roy, and A. Pérennec, "Application of negative group delay active circuits to the design of broadband and constant phase shifters," *Microw. Opt. Technol. Lett.*, vol. 50, no. 12, pp. 3078–3080, Dec. 2008.

[2] H. Mirzaei and G. V. Eleftheriades, "Arbitrary-angle squint-free beamforming in series-fed antenna arrays using non-foster elements synthesized by negative-group-delay networks," *IEEE Trans. Antennas Propag.*, vol. 63, no. 5, pp. 1997–2010, May 2015.

[3] H. Choi, Y. Jeong, C. Dong Kim, and J. S. Kenney, "Efficiency enhancement of feedforward amplifiers by employing a negative group-delay circuit," *IEEE Trans. Microw. Theory Techn.*, vol. 58, no. 5, pp. 1116–1125, May 2010.

[4] Y. K. G. Hau, V. Postoyalko, and J. R. Richardson, "Design and characterization of a microwave feed-forward amplifier with improved wide-band distortion cancellation," *IEEE Trans. Microw. Theory Techn.*, vol. 49, no. 1, pp. 200–203, Jan. 2001.

[5] G. Chaudhary and Y. Jeong, "A design of power divider with negative group delay characteristics," *IEEE Microw. Wireless Compon. Lett.*, vol. 25, no. 6, pp. 394–396, Jun. 2015.

[6] S. Lucyszyn and I. D. Robertson, "Analog reflection topology building blocks for adaptive microwave signal processing applications," *IEEE Trans. Microw. Theory Techn.*, vol. 43, no. 3, pp. 601–611, Mar. 1995.

[7] C. D. Broomfield and J. K. A. Everard, "Broadband negative group delay networks for compensation of microwave oscillators and filters," *Electron. Lett.*, vol. 36, no. 23, pp. 1931–1933, Nov. 2000.

[8] M. W. Mitchell and R. Y. Chiao, "Negative group delay and 'fronts' in a causal system: An experiment with very low frequency bandpass amplifiers," *Phys. Lett. A*, vol. 230, nos. 3–4, pp. 133–138, Jun. 1997.

[9] M. Kitano, T. Nakanishi, and K. Sugiyama, "Negative group delay and superluminal propagation: An electronic circuit approach," *IEEE J. Sel. Topics Quantum Electron.*, vol. 9, no. 1, pp. 43–51, Jan. 2003.

[10] F. Wan, N. Li, B. Ravelo, Q. Ji, B. Li, and J. Ge, "The design method of the active negative group delay circuits based on a microwave amplifier and an RL-series network," *IEEE Access*, vol. 6, pp. 33849–33858, 2018.

[11] F. Wan, N. Li, B. Ravelo, J. Ge, and B. Li, "Time-domain experimentation of NGD ActiveRC-network cell," *IEEE Trans. Circuits Syst. II, Exp. Briefs*, vol. 66, no. 4, pp. 562–566, Apr. 2019.

[12] B. Ravelo, A. Pérennec, M. Le Roy, and Y. G. Boucher, "Active microwave circuit with negative group delay," *IEEE Microw. Wireless Compon. Lett.*, vol. 17, no. 12, pp. 861–863, Dec. 2007.

[13] M. Kandic and G. E. Bridges, "Asymptotic limits of negative group delay in active resonator-based distributed circuits," *IEEE Trans. Circuits Syst. I, Reg. Papers*, vol. 58, no. 8, pp. 1727–1735, Aug. 2011.

[14] F. Wan, N. Li, B. Ravelo, Q. Ji, and J. Ge, "S-parameter model of three parallel interconnect lines generating negative group-delay effect," *IEEE Access*, vol. 6, pp. 57152–57159, Oct. 2018.

[15] Y. Wu, H. Wang, Z. Zhuang, Y. Liu, Q. Xue, and A. A. Kishk, "A novel arbitrary terminated unequal coupler with bandwidth-enhanced positive and negative group delay characteristics," *IEEE Trans. Microw. Theory Techn.*, vol. 66, no. 5, pp. 2170–2184, May 2018.
[16] G. Chaudhary and Y. Jeong, "Low signal-attenuation negative group-delay network topologies using coupled lines," *IEEE Trans. Microw. Theory Techn.*, vol. 62, no. 10, pp. 2316–2324, Oct. 2014.
[17] H.-Y. Yao, N. C. Chen, T.-H. Chang, and H. G. Winful, "Tunable negative group delay in a birefringent Fabry–Pérot-like cavity with high fractional advancement induced by cross-interference effect," *IEEE Trans. Microw. Theory Techn.*, vol. 64, no. 10, pp. 3121–3130, Oct. 2016.
[18] B. Ravelo, "Negative group-delay phenomenon analysis with distributed parallel interconnect line," *IEEE Trans. Electromagn. Compat.*, vol. 58, no. 2, pp. 573–580, Apr. 2016.
[19] B. Ravelo, "Theory of coupled line coupler-based negative group delay microwave circuit," *IEEE Trans. Microw. Theory Techn.*, vol. 64, no. 11, pp. 3604–3611, Nov. 2016.
[20] S. Sattel. *What is High Speed PCB Design?* Accessed: Mar. 26, 2020. [Online]. Available: https://www.autodesk.com/products/eagle/blog/high-speed-pcb-design/
[21] C.-T.-M. Wu and T. Itoh, "Maximally flat negative group-delay circuit: A microwave transversal filter approach," *IEEE Trans. Microw. Theory Techn.*, vol. 62, no. 6, pp. 1330–1342, Jun. 2014.
[22] G. Chaudhary, Y. Jeong, and J. Lim, "Microstrip line negative group delay filters for microwave circuits," *IEEE Trans. Microw. Theory Techn.*, vol. 62, no. 2, pp. 234–243, Feb. 2014.
[23] Z. Wang, Y. Cao, T. Shao, S. Fang, and Y. Liu, "A negative group delay microwave circuit based on signal interference techniques," *IEEE Microw. Wireless Compon. Lett.*, vol. 28, no. 4, pp. 290–292, Apr. 2018.
[24] H. Choi, Y. Jeong, J. Lim, S.-Y. Eom, and Y.-B. Jung, "A novel design for a dual-band negative group delay circuit," *IEEE Microw. Wireless Compon. Lett.*, vol. 21, no. 1, pp. 19–21, Jan. 2011.
[25] G. Chaudhary, Y. Jeong, and J. Lim, "Miniaturized dual-band negative group delay circuit using dual-plane defected structures," *IEEE Microw. Wireless Compon. Lett.*, vol. 24, no. 8, pp. 521–523, Aug. 2014.
[26] H. Taher and R. Farrell, "Dual wide-band miniaturized negative group delay circuit using open circuit stubs," *Microw. Opt. Technol. Lett.*, vol. 60, no. 2, pp. 428–432, Feb. 2018.
[27] T. Shao, S. Fang, Z. Wang, and H. Liu, "A compact dual-band negative group delay microwave circuit," *Radioengineering*, vol. 27, no. 4, pp. 1070–1076, Dec. 2018.

FAYU WAN (Member, IEEE) was received the Ph.D. degree in electronic engineering from the University of Rouen, Rouen, France, in 2011. From 2011 to 2013, he was a Postdoctoral Fellow with the Electromagnetic Compatibility Laboratory, Missouri University of Science and Technology, Rolla. He is currently a Full Professor with the Nanjing University of Information Science and Technology, Nanjing, China. His current research interests include negative group delay circuits, electrostatic discharge, electromagnetic compatibility, and advanced RF measurement.

BIN LIU received the B.Sc. degree in information engineering from the Xuhai College, China University of Mining and Technology, Xuzhou, China, in 2019. He is currently pursuing the M.S. degree with the Nanjing University of Information Science and Technology, Nanjing, China. His research interests include electrostatic discharge and electromagnetic compatibility.

PREETI THAKUR received the M.Phil. and Ph.D. degrees from Himachal Pradesh University (HPU), Shimla. She has published more than 100 research articles in national and international journals. She has supervised 66 master's and four Ph.D. students. She is currently working as a Professor and the Head of the Physics Department, Amity University Haryana. She is invited by the Royal Academy of Engineering U.K., to attend Invited Professors meet at Birmingham. She has several national and international collaborations and projects. She has filed 14 patents till date. She is the Gold Medalist in electronics from HPU.

ATUL THAKUR received the M.Sc., M.Phil., and Ph.D. degrees from Himachal Pradesh University, Shimla, the Ph.D. degree from the University of Brest, France, and the Ph.D. degree from National Taiwan University, Taiwan. He has worked on various projects sponsored by DRDO, DAE, DST, and MNRE. He is currently working as the Director of the Centre for Nanotechnology, Amity University Haryana. He has published more than 100 international research articles and filed 15 Patents. He has been awarded the Newton Award from Royal Academy of Engineering, U.K.

SÉBASTIEN LALLÉCHÈRE (Member, IEEE) was born in Nevers, France, in 1979. He received the M.Sc. degree from Polytech Clermont and the Ph.D. degree from Universite Blaise Pascal, Clermont-Ferrand, France, in 2002 and 2006, respectively, in computational modeling and electronics/electromagnetism.

He has served as a Research Engineer from LASMEA, Clermont-Ferrand, in 2007, focusing on intensive computational methods for electromagnetics. He is currently an Associate Professor with Institut Pascal and Universite Clermont Auvergne, Clermont-Ferrand. His research interests include the fields of electromagnetic compatibility, including antennas and propagation, complex and reverberating electromagnetic environments, electromagnetic coupling, computational electromagnetics, stochastic modeling, and sensitivity analysis in electrical engineering.

WENCESLAS RAHAJANDRAIBE (Member, IEEE) received the B.Sc. degree in electrical engineering from Nice Sophia-Antipolis University, France, in 1996, the M.Sc. degree (Hons.) in electrical engineering from the Science Department, University of Montpellier, France, in 1998, and the Ph.D. degree in microelectronics form the University of Montpellier. Since 1998, he has been with the Microelectronics Department of Informatics, Robotics, and the Microelectronics Laboratory of Montpellier (LIRMM). Since 2003, he has also been with the Microelectronic Department of Materials, Microelectronics, and the Nanoscience Laboratory of Provence (IM2NP), Marseille, France, where he was an Associate Professor. Since 2014, he has also been a Professor with Aix Marseille University, where he also heads the IM2NP Laboratory, Integrated Circuit Design Group. He is currently a Full Professor with the University of Aix-Marseille. His research is focused on the design of Analog and RF IC's for telecommunication systems and for smart sensor ultra-low power IC interfaces. He has served on program committees of the IEEE NEWCAS and ICECS. He has been and is a Reviewer of contributions submitted to several IEEE conferences and journals, such as ISACS, NEWCAS, MWSCAS, ESSCIRC, ESSDERC, RFIC, and the TRANSACTIONS ON CIRCUITS AND SYSTEMS—I and II.

BLAISE RAVELO (Member, IEEE) is currently a University Full Professor with NUIST, Nanjing, China. His research interest is on multiphysics and electronics engineering. He is also a Pioneer of the Negative Group Delay (NGD) concept about $t < 0$ signal travelling physical space. This extraordinary concept is potentially useful for anticipating and prediction all kind of information. He was a Research Director of nine Ph.D. students (seven defended), Postdoctoral Researchers, research engineers, and Master internships. With USA, Chinese, Indian, European, and African partners, he is also actively involved and contributes on several international research projects (ANR, FUI, FP7, INTERREG, H2020, Euripides^2, Eurostars…). He is a member of *IET Electronics Letters* Editorial Board as circuit and system subject editor. He has been a member of scientific technical committee of Advanced Electromagnetic Symposium (AES), since 2013. His Google scholar H-index in 2020 is 20. He is a member of research groups: the IEEE, URSI, GDR Ondes, Radio Society and coauthors of more than 250 scientific research articles in new technologies published in international conferences and journals. He is a Lecturer on circuit and system theory, science, technology, engineering, and maths (STEM) and applied physics. He is regularly invited to review articles submitted for publication to international journals the IEEE TRANSACTIONS ON MICROWAVE THEORY AND TECHNIQUES, the IEEE TRANSACTIONS ON CIRCUITS AND SYSTEMS, the IEEE TRANSACTIONS ON ELECTROMAGNETIC COMPATIBILITY, the IEEE TRANSACTIONS ON INDUSTRIAL ELECTRONICS, IEEE ACCESS, *IET CDS*, and *IET MAP*, and books (Wiley and Intech Science).